8-28-2014

In situ TEM study on the microstructural evolution during electric fatigue in 0.7Pb(Mg1/3Nb2/3)O3–0.3PbTiO3 ceramic

Hanzheng Guo
Iowa State University

Xiaoli Tan
Iowa State University, xtan@iastate.edu

Shujun Zhang
Pennsylvania State University

In situ TEM study on the microstructural evolution during electric fatigue in 0.7Pb(Mg1/3Nb2/3)O3–0.3PbTiO3 ceramic

Abstract

In this work, we report an experimental technique with nanometer resolution to reveal the microstructural mechanism for electric fatigue in ferroelectrics. The electric field in situ transmission electron microscopy (TEM) was used to directly visualize the domain evolution during the fatigue process in a 0.7Pb(Mg1/3Nb2/3)O3–0.3PbTiO3 ceramic. The structure–property relationship was well demonstrated by combining the microscopic observations with corresponding dielectric, piezoelectric, and ferroelectric properties measured on bulk specimens. It was found that the domain switching capability was substantially suppressed after 103 cycles of bipolar fields, leading to an immobilized domain configuration thereafter. Correspondingly, a pronounced degradation of the functionality of the ceramic was manifested, accompanying with a coercive field bumping and polarization current density peak broadening. The reduction of the polarization, dielectric constant, and piezoelectric coefficient were found to follow a power-law relation. Seed inhibition mechanism was suggested to be responsible for the observed fatigue behaviors.

Disciplines

Ceramic Materials | Electronic Devices and Semiconductor Manufacturing | Structural Materials

Comments

This article is from *Journal of Materials Research* (2014): 1, doi:10.1557/jmr.2014.228. Posted with permission.

In situ TEM study on the microstructural evolution during electric fatigue in $0.7Pb(Mg_{1/3}Nb_{2/3})O_3$–$0.3PbTiO_3$ ceramic

Hanzheng Guo[a] and Xiaoli Tan
Department of Materials Science and Engineering, Iowa State University, Ames, Iowa 50011, USA
Shujun Zhang
Materials Research Institute, Pennsylvania State University, University Park, Pennsylvania 16802, USA

(Received 13 June 14; accepted 6 August 14)

In this work, we report an experimental technique with nanometer resolution to reveal the microstructural mechanism for electric fatigue in ferroelectrics. The electric field in situ transmission electron microscopy (TEM) was used to directly visualize the domain evolution during the fatigue process in a $0.7Pb(Mg_{1/3}Nb_{2/3})O_3$–$0.3PbTiO_3$ ceramic. The structure–property relationship was well demonstrated by combining the microscopic observations with corresponding dielectric, piezoelectric, and ferroelectric properties measured on bulk specimens. It was found that the domain switching capability was substantially suppressed after 10^3 cycles of bipolar fields, leading to an immobilized domain configuration thereafter. Correspondingly, a pronounced degradation of the functionality of the ceramic was manifested, accompanying with a coercive field bumping and polarization current density peak broadening. The reduction of the polarization, dielectric constant, and piezoelectric coefficient were found to follow a power-law relation. Seed inhibition mechanism was suggested to be responsible for the observed fatigue behaviors.

I. INTRODUCTION

Electric fatigue has been an ongoing research topic in ferroelectric communities for several decades due to the technological importance and extensive application of ferroelectric-based devices such as nonvolatile memories, field-effect transistors, ferroelectric tunneling junctions, transducers, and actuators.[1–8] A fingerprint of electric fatigue in ferroelectric oxides is the degradation of their functionality (e.g., switchable polarization) during repetitive polarization switching.[9,10] It has severely hindered the long-term operation and reliability of ferroelectric materials. Throughout the past half-century, a large body of experimental and theoretical studies has been conducted to investigate the origin of electric fatigue.[1,9,10] Several phenomenological scenarios and microscopic mechanisms have been proposed such as electrode degradation,[9] near-electrode passive layer formation,[11] nucleation inhibition,[12] domain wall pinning,[13] and local phase decomposition.[14] However, a consensus has not been reached due to the complex nature of the fatigue process.[1,9]

As is well known, the polarization state and polarization switching in ferroelectric crystals are intrinsically linked to ferroelectric domain arrangements and their transformations. Essentially, ferroelectric domains dictate the dielectric, piezoelectric, and ferroelectric properties for ferroelectric crystals. Thus, direct imaging of domain evolution during electric cycling is critical to elucidate the underlying mechanisms for electric fatigue. Unfortunately, a vast majority of previous fatigue studies have mainly focused on macroscopic property measurements without microscopic pictures.[9,10,15,16] Until now, very limited techniques, such as piezoresponse force microscopy (PFM)[17–23] and x-ray microdiffraction,[24] were developed to provide microscopic insight for electric fatigue. However, the application of these probing tools is still restricted by technical challenges. For example, PFM only recorded top morphology change during fatigue and was not able to monitor crystal structure evolutions.[17–23] It is now understood that both macroscopic properties and microscopic morphologies are significantly influenced by structural phase transitions.[25–30] For x-ray microdiffraction, high spatial resolution is still not approachable when the length scale is reduced to individual grain level and multidomain structures are presented within. To circumvent these technical hindrances effectively and obtain a comprehensive understanding of electric fatigue from a microscopic viewpoint, electric field in situ transmission electron microscopy (TEM)[31–35] is used and extended by applying an AC electric field in this study.

The in situ TEM technique has been demonstrated to be a powerful probing tool for investigating microstructural origins of functionality (e.g., the piezoelectricity) evolution under electric field.[25–30] Domain morphology transformations over a length scale from micrometers to nanometers can be effectively recorded due to its

[a]Address all correspondence to this author.
e-mail: ghanzheng@gmail.com
DOI: 10.1557/jmr.2014.228

high resolution. Simultaneously, crystal structures evolution can also be monitored by electron diffraction patterns, especially when phase variants are inferred by superlattice diffractions.[25,27] Our previous in situ TEM studies have focused on the microstructural response to the DC electric field.[25–30] Here, microstructures evolution during a bipolar fatigue process was directly visualized using an electric field in situ TEM technique. Polycrystalline $0.7Pb(Mg_{1/3}Nb_{2/3})O_3$–$0.3PbTiO_3$ (0.7PMN-0.3PT) ceramic was used for the demonstration. In situ observations combined with dielectric, piezoelectric, and ferroelectric properties measurements on bulk specimens eventually allow for elucidation of the underlying mechanism for electric fatigue in 0.7PMN-0.3PT.

II. EXPERIMENTAL

A. Ceramic preparation

The $0.7Pb(Mg_{1/3}Nb_{2/3})O_3$–$0.3PbTiO_3$ ceramic (TRS Ceramics, State College, PA) was synthesized through the columbite precursor method.[36] $MgNb_2O_6$ was prepared by the reaction $MgO + Nb_2O_5 \rightarrow MgNb_2O_6$ at 1200 °C for 4 h. After dry-milling and passing through 100 mesh sieve, the columbite powder slurry was further milled with a high-energy attritor-mill for 6 h. Then, $PbCO_3$ and TiO_2 were added to the columbite powder and vibratory-milled for 18 h. The mixture was dried and then calcined at 700 °C for 4 h. This powder was ground and passed through 80 mesh, then attritor-milled for 8 h. With acrylic resin as a binder, the calcined powder was biaxially pressed into 76 mm × 50 mm × 50 mm blocks. The green bodies were sintered at 1250 °C for 3 h in alumina crucibles with $PbZrO_3$ source powder to maintain a PbO atmosphere. After sintering, the blocks were hot isostatically pressed at 1150 °C for 2 h in an O_2/Ar atmosphere.

B. Fatigue measurements on bulk specimen

The fatigue experiment was performed on bulk specimen by applying a bipolar triangular waveform with a frequency of 2 Hz and a peak field of 20 kV/cm. Silver films were sputtered to serve as electrodes. Macroscopic properties were measured for various cycling intervals. For ferroelectric characterizations, the polarization (P) versus electric field (E) hysteresis loops were measured using a standardized ferroelectric test system (RT-66A, Radiant Technologies, Albuquerque, NM) at 4 Hz at room temperature. The polarization current density J was determined by taking the derivative of polarization with respect to time, i.e., $dP(t)/dt$. For piezoelectric measurements, the piezoelectric coefficient d_{33} was measured by a piezo-d_{33} meter (Model ZJ-4B, Institute of Acoustics, Chinese Academy of Science, China) to take 10 measurements across the electrode of the sample. The room temperature dielectric constant was measured using an LCR meter (HP-4284A, Hewlett-Packard, Palo Alto, CA) at a frequency of 1 kHz.

C. In situ TEM study

For electric field in situ TEM experiments, disk specimens (3 mm in diameter) were prepared from ceramic pellets through standard procedures including grinding, cutting, dimpling, and ion milling. The dimpled disks were annealed at 300 °C for 2 h to minimize the residual stresses before Ar-ion milling to the point of electron transparency. In situ TEM experiments were carried out on a Philips CM-30 microscope (Philips, Amsterdam, Holland) operated at 200 kV. The detailed experimental setup can be found in our previous reports.[31–35] After the initial poling process (a DC field applied at the very first quarter cycle) from its virgin state, a bipolar cycling with a frequency of 10 Hz and a peak field of 10 kV/cm was applied. TEM micrographs were recorded at zero field after certain cycles were made. In this study, only the nominal electric field (the applied voltage divided by the electrode spacing) is cited for the in situ TEM results. However, it should be noted that the TEM specimen has a central perforation which intensifies the actual field in the target grains.[31,37] In the present case, an intensification ratio of 2 is considered for the actual field strength due to the circular-shaped geometry of the perforation.[31,37] Therefore, for the fatigue measurements mentioned in Sec. II. B on bulk specimens, an amplitude of 20 kV/cm was applied during the bipolar electric cycling.

III. RESULTS AND DISCUSSION

A. Domain morphology in the virgin state

The crystalline solution $(1-x)$PMN-xPT is known to have a systematic domain structure evolution when the phase variant evolves with $PbTiO_3$ content.[38–40] For tetragonal phase compositions ($x > 0.35$), normal micrometer-sized lamellar domains were observed[38–40]; whereas for rhombohedral phase compositions ($x \sim 0.25$–0.3), miniaturized polar nanodomains were found to form spindle-like domain features.[39,40] Between these two ($x \sim 0.3$–0.35), a morphotropic phase boundary (MPB) with a monoclinic phase was present to bridge the tetragonal and rhombohedral structures.[38,39,41,42] Correspondingly, a hierarchical domain pattern with the micrometer-sized lamellar-type consisting of cross-hatched nanodomains inside was adopted.[38,39,42–44] This typical domain configuration was commonly observed for both single crystals and polycrystalline ceramics at, or in the vicinity of the MPB.[38–40,42–44] In the present study, a consistent observation was also obtained in the 0.7PMN-0.3PT polycrystalline ceramic. As shown in Fig. 1, for a representative grain along its [113] zone axis in the virgin state 0.7PMN-0.3PT ceramic, the typical hierarchy domain feature was clearly

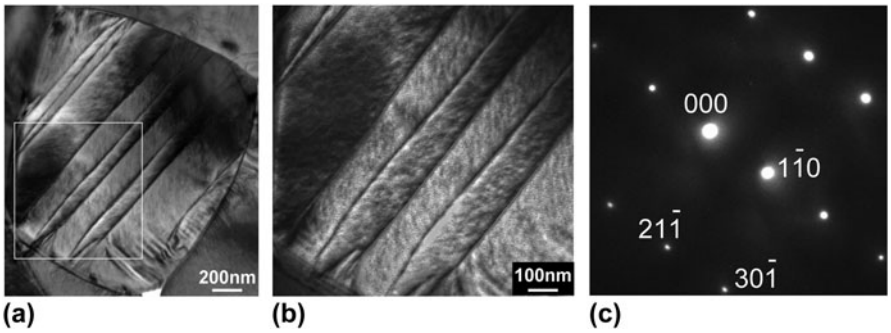

FIG. 1. (a) Bright-field micrograph of a representative grain along its [113] zone axis in the virgin state of 0.7PMN-0.3PT ceramic. (b) Higher magnification image of the boxed area in (a) to show the hierarchical domain structure. (c) The corresponding selected area diffraction pattern.

demonstrated: the micrometer-sized $(1\bar{1}0)$ lamellar domains were manifested with two traces of tweed-like nanodomains coexisting inside. These nanodomains were found roughly along two $\langle 30\bar{1}\rangle$ directions, and crosshatched with each other to form a substructure.

B. Domain morphology evolution during fatigue

Microstructure evolution under electric process in 0.7PMN-0.3PT ceramic is exemplified in Fig. 2 by a [001]-aligned grain. Prior to the cycling, the domain morphology evolution during the first quarter cycle (referred to as "initial poling" hereafter) was initially shown in Figs. 2(a)–2(c). In the virgin state [Fig. 2(a)], two sets of orthogonal lamellar domains were clearly observed and found parallel to the {110} planes. Inside these micrometer-sized domains, nanodomains were also manifested. However, they became nearly invisible due to their extremely weak contrast at lower magnifications, as can be seen in Fig. 1(a). When the electric field reached 6 kV/cm, apparent domain switching was noted. Some portions of the $(\bar{1}10)$ domains were consumed by the other set of (110) domains. Further increasing the electric field to 10 kV/cm facilitated the consummation process, and finally the entire grain was occupied by the (110) domains. In addition, large domain mixed with thin domain striations were also formed at the far left side of the grain during this domain alignment process. Domain evolution during initial poling was found to be irreversible. The configuration of the poled state remained unchanged upon removal of the poling field.

Electric reversals were then carried out by repetitively applying bipolar cycles at a nominal amplitude of 10 kV/cm. It is interesting to note that after 20 cycles a substructure with nanometer-sized domain traces developed within the lamellar domains and formed a herringbone type of domain configuration [Fig. 2(d)]. Those confined short domains appeared to have domain walls along (010) and (100) planes. Also, the far left part of this grain split into a cluster of [010]-aligned thin domain strings. Upon further cycling, domain switching proceeded. As shown in Fig. 2(e), for the end-state after 10^3 cycles some portion of nanodomain traces disappeared, but still with some portion preserved and mixed with lamellar domains. Additionally, some newly formed defects were observed, as roughly aligned along the bright arrow indicated in Fig. 2(e). It has been known that structural imperfections are generated in fatigued ferroelectrics.[45–48] For the defects in Fig. 2(e), they might be oxygen vacancy clusters[45,46] or dislocations.[47,48] After 10^3 cycles, nearly all the domains became incapable of switching with further cycling, leading to a frozen configuration after fatigue. In addition to these immobilized domains, some inhibited small domains seem to have appeared at the grain boundary in the lower part in Fig. 2(e). On the other hand, the crystal structure was also monitored by the electron diffraction pattern during the initial poling and fatigue process. No noticeable changes were found compared with the virgin state pattern [Fig. 2(f)].

Fatigue-induced domain freezing under the influence of electric reversals in 0.7PMN-0.3PT was reproducibly observed, as shown by another grain along its [112] zone axis in the same TEM specimen (Fig. 3). The first three micrographs [Figs. 3(a)–3(c)] still show microstructural evolution during initial poling. In the virgin state [Fig. 3(a)], in addition to the tweed-like fine domain clusters, micrometer-sized lamellar domains lying on the $(1\bar{1}0)$ crystallographic planes were observed. When the electric field was increased to 5 kV/cm, the large lamellar domains at the upper-right corner were transformed into thin-aligned striation-like domains with traces along the $[1\bar{1}0]$ direction [Fig. 3(b)]. At 10 kV/cm, the domain striations became predominant, as manifested by the disappearance of the large lamellar domains and the occurrence of another set of $[3\bar{1}\bar{1}]$-aligned fine traces [Fig. 3(c)]. During the fatigue process, an apparent alteration of domain morphology was observed before 10^3 cycles. As exemplified in Fig. 3(d), a significant portion of $[1\bar{3}1]$-aligned domain striations were induced after 20 cycles, leading to a condensed domain configuration for the entire grain. When the cycling numbers

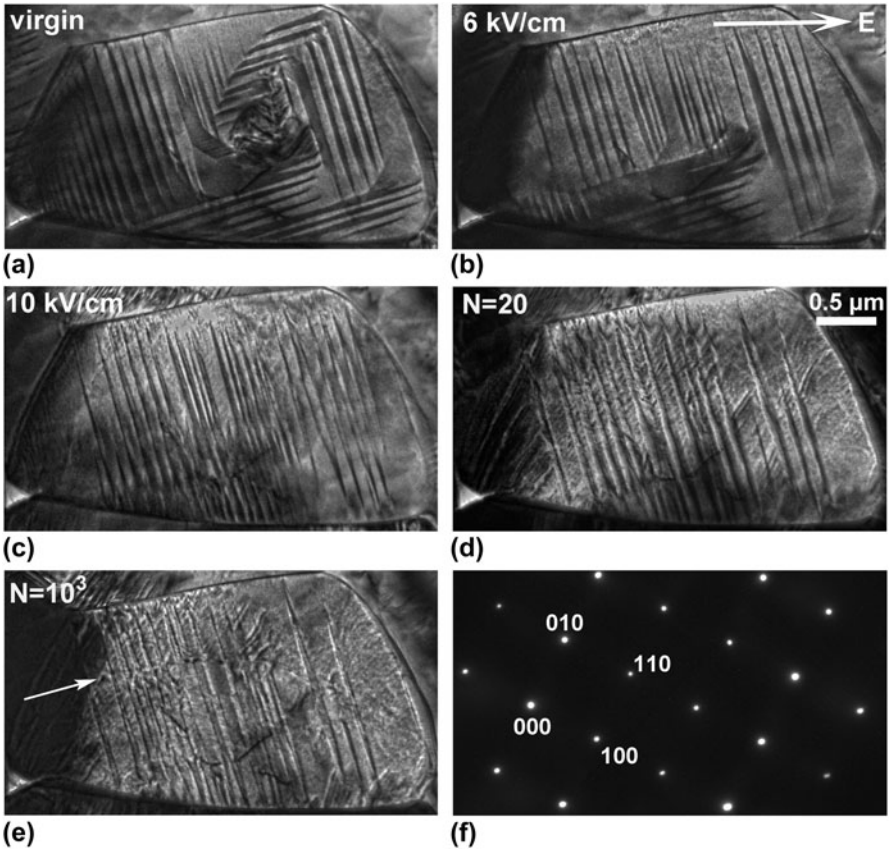

FIG. 2. In situ TEM observations of a grain along its [001] zone axis in a 0.7PMN-0.3PT specimen during initial poling and bipolar electric reversals. Bright-field micrographs at (a) virgin state, (b) 6 kV/cm, and (c) 10 kV/cm during initial poling; (d) after 20 cycles and (e) after 10^3 cycles of bipolar cycling with a nominal amplitude of 10 kV/cm. The produced defects after 10^3 cycles are marked roughly along the direction of the bright arrow shown in (e). The selected area diffraction pattern recorded at the virgin state is shown in (f). The positive direction of applied fields in the TEM experiment is indicated by the bright arrow in (b). No apparent changes in the electron diffraction pattern are noticed during initial poling and fatigue process.

increased to 10^3, most of the well-defined domain striations were gradually transformed into fine domain traces and large domain areas [Fig. 3(e)]. With further increase of electric reversals, most of the domains were found inactive to the electric stimulus; the switching ability of the domains was substantially impeded. Only minor switching was noticed after 10^4 cycles [Fig. 3(f)], and eventually the grain was dominated by an immobilized domain configuration [Fig. 3(g)]. The frozen domain morphology remained even when a much higher DC field of −31 kV/cm was applied [Fig. 3(h)]. Again, the electron diffraction pattern of the virgin state [Fig. 3(i)] stayed unchanged during the initial poling and fatigue process.

C. Impact on macroscopic properties

To correlate the fatigue-induced microstructural evolution to macroscopic properties, measurements on dielectric, piezoelectric, and ferroelectric properties were carried out on bulk ceramic specimen. A well-illustrated structure–property relationship was established. As shown in Figs. 4 and 5, a degradation of dielectric, piezoelectric, and ferroelectric properties was manifested, which was similar to the fatigue behavior of lead-based thin films, as reported in previous literature.[49–52]

Figure 4 depicted the polarization hysteresis and corresponding polarization current density evolutions during fatigue. As can be seen, an apparent fatigue behavior was manifested by a reduction of remnant polarization (P_r) as well as an increase in coercive field (E_C) upon electric reversals [Fig. 4(a)], while corresponding polarization current density (J) peaks became lower and broadened [Fig. 4(b)]. Moreover, splitting of the current density peaks was found during the fatigue process.[53,54] It is interesting to notice that electric reversal from the virgin state ($N = 1$) has only one very sharp and narrow current density peak, suggesting a direct 180° reversal at the very first cycle. After that, doublets were seen on the two peaks (see cycle 3 and 10^3 curves). This may suggest that the polarization reversal occurred through a multistep process.[19,55–60] Further cycling smeared out the doublets and broadened the two peaks. This appears to indicate that the reversal process takes place within a wide field range due to severe domain freezing.

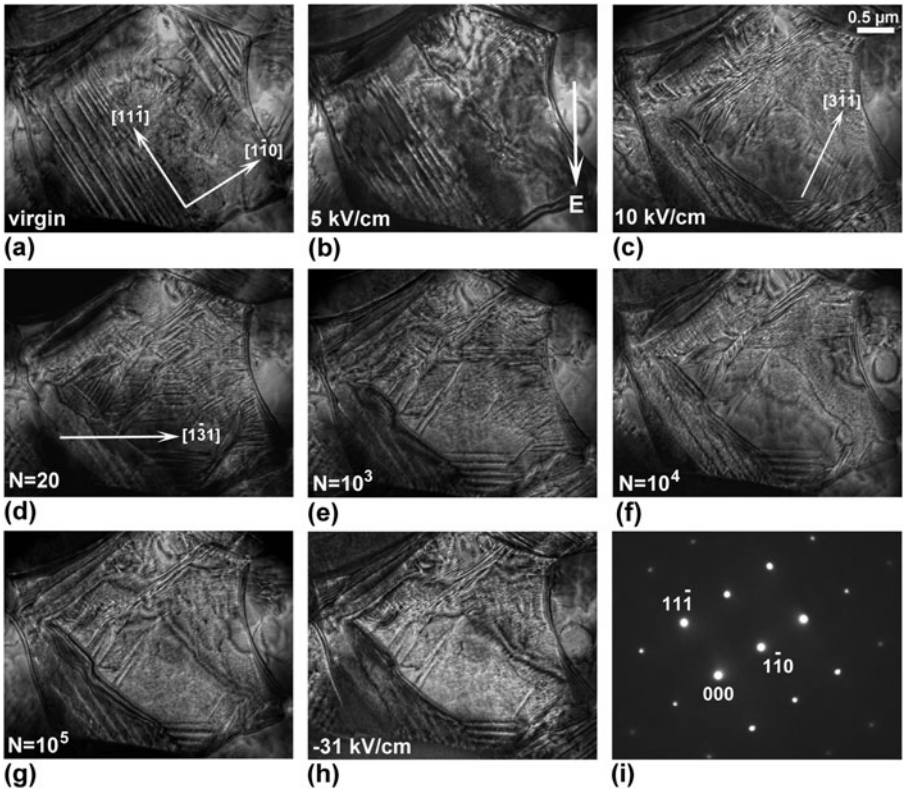

FIG. 3. In situ TEM observations of another grain along its [112] zone axis in the same 0.7PMN-0.3PT specimen during initial poling and electric reversals. Bright-field micrographs at (a) virgin state, (b) 5 kV/cm, and (c) 10 kV/cm during initial poling; (d) after 20 cycles, (e) after 10^3 cycles, (f) after 10^4 cycles, and (g) after 10^5 cycles during fatigue. After fatigue, the grain shown in (g) was further stressed at −31 kV/cm, as displayed in (h). The selected area diffraction pattern recorded at the virgin state is shown in (i). The positive direction of applied fields in the TEM experiment is indicated by the bright arrow in (b). No apparent changes in the electron diffraction pattern are noticed during initial poling and fatigue process.

Generally, the degradation of remnant polarization (P_r) and maximum polarization (P_m) is an indication of electric fatigue in ferroelectric properties.[9,10] Both of them describe the amount of domains that can be effectively switched under electric field. However, the coercive field is usually used to characterize how difficult domain switching becomes when electric field direction is reversed. As summarized in Fig. 5(a), both polarization and coercive field followed a plateau trend and changed slightly before 10^3 cycles. Remarkable polarization decay was observed thereafter, accompanied by a bump up of the coercive field. Quantitatively, P_m and P_r showed a similar degradation to 79.8% and 80.0% of their original values after 10^4 cycles, respectively, whereas E_C increased to 167.1% of its initial value. For dielectric and piezoelectric properties, as characterized by dielectric constant (ε_r) and piezoelectric coefficient (d_{33}), the overall evolution followed the same reduction trend as the polarization: the dielectric constant and piezoelectric coefficient remained 93.8% and 92.0% of their original values after 10^3 cycles, respectively, but significantly dropped to 55.3% and 50.0% after 10^4 cycles.

For classic ferroelectrics, such as Pb(Zr,Ti)O_3 and $BiFeO_3$, the fatigue behavior usually exhibits a nonlinear decay by plotting remnant polarization with respect to logarithm of electric reversals.[10] Obtained fatigue profiles are generally fitted by functions like $P_r \propto N^{-1/4}$, $P_r \propto (aN + 1)^{-m}$, or $P_r \propto A + \exp(-aN)$.[9,61] Typically, a plateau stage of slow reduction is initially observed, followed by a sharp decay and subsequent logarithmic stage.[10] In this study, a similar fatigue behavior was also observed, as demonstrated by a stable stage within the initial 10^3 cycles and a fast decay stage thereafter. These macroscopic behaviors were well correlated to the in situ TEM observations, where the domains remained actively switched within the initial 10^3 cycles and were progressively frozen thereafter. The degradation profile for the macroscopic properties can be well fitted by the power-law $P_r \propto (aN + 1)^{-m}$ relation.[9,61] The fitting curves (solid lines in Fig. 5) are shown as the following, where P_{r0}, P_{m0}, d_0, and ε_{r0} are parameters of denoting the unfatigued state; N is the cycle number; a is the fitting constant; and m is the decay constant which characterizes the speed of the fatigue.

$$P_r(N) = P_{r0}(aN + 1)^{-m} \quad , \qquad (1)$$

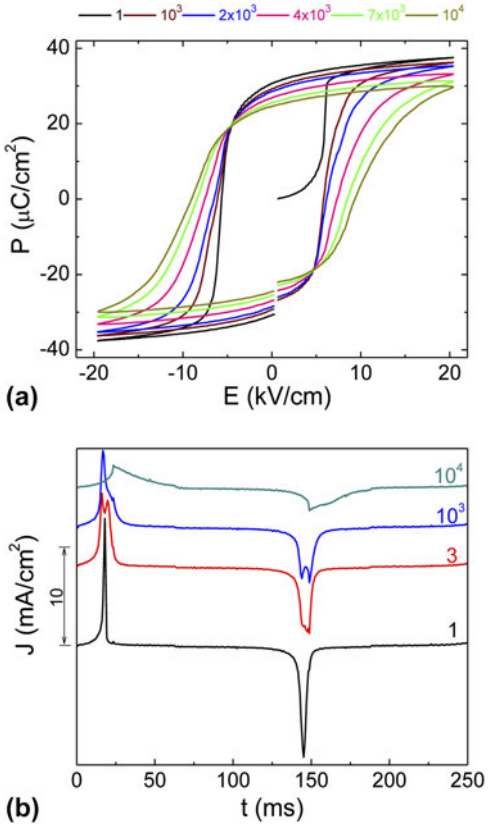

FIG. 4. (a) Change of the polarization hysteresis loop and (b) polarization current density curves during electric fatigue in 0.7PMN-0.3PT bulk ceramic.

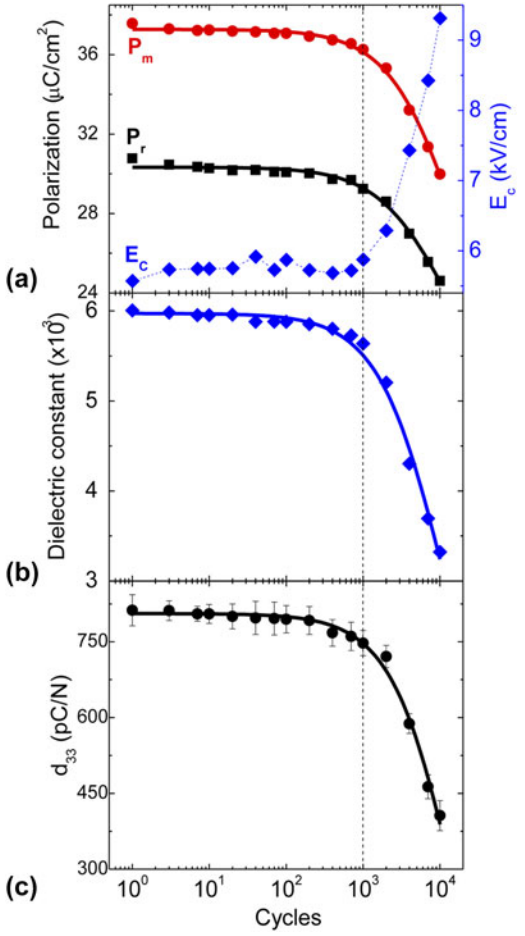

FIG. 5. (a) Polarization and coercive field, (b) dielectric constant, and (c) piezoelectric coefficient as a function of cycling number measured from the same bulk specimen as in Fig. 4. The experimentally measured results are shown as discrete points, while the solid fitting curves are derived using the power-law relation. The fitting equations are shown in the text.

with $P_{r0} = 30.330\ \mu C/cm^2$, $a = 2.067 \times 10^{-4}$, and $m = 0.188$.

$$P_m(N) = P_{m0}(aN+1)^{-m} \quad , \tag{2}$$

with $P_{m0} = 37.274\ \mu C/cm^2$, $a = 1.164 \times 10^{-4}$, and $m = 0.286$.

$$d_{33}(N) = d_0(aN+1)^{-m} \quad , \tag{3}$$

with $d_0 = 805.928$ pC/N, $a = 1.184 \times 10^{-5}$, and $m = 6.517$.

$$\varepsilon_r(N) = \varepsilon_{r0}(aN+1)^{-m} \quad , \tag{4}$$

with $\varepsilon_{r0} = 5972.600$, $a = 8.448 \times 10^{-5}$, and $m = 0.999$.

D. Discussion

It has been shown that electric fatigue in ferroelectric oxides is a complicated process, and both intrinsic and extrinsic contributions devote to the reduction of switchable polarization.[1,9,10] During the past several decades of intensive studies, various models have been proposed, for example, electrode degradation, passive layer formation, domain wall pinning, and seed inhibition.[1,9,10] According to Tagantsev et al.,[9] these mechanisms can be phenomenologically distinguished based on different fatigue behaviors: for the electrode degradation model, polarization parameters of the *P*–*E* loop (e.g., P_r and P_m) and the small-signal dielectric constant are supposed to scale down by the same factor.[9] However, this is not the case here because the notable difference of the decay constant *m* has been demonstrated for all parameters [see Eqs. (1), (2), and (4)]. The cycling-driven formation of the near-electrode passive layer should be manifested by a strong tilt of the polarization hysteresis loop, whereas the coercive field is either not influenced or slightly decreased.[9] This expectation is inconsistent with the remarkable bumping of the coercive field in the present study. For domain wall pinning and seed inhibition mechanisms, both cases show the frozen domain configuration after fatigue. For the former scenario, the domain walls are pinned due to their interaction with the charged defects, while for the later one the nucleation seeds for the reversed

domains are blocked in their embryonic state before they can create a macroscopic domain.[9] However, these two mechanisms can still be experimentally distinguished from each other. The essential feature of the domain wall pinning is the dense domain structure.[9] A clear manifestation of the fatigued state induced by this mechanism should be demonstrated by a high concentration of immobilized domain walls. As a consequence, the small-signal dielectric constant is expected to increase.[9] In contrast, the fatigued state created by the seed inhibition mechanism generally contains relatively large domain regions, yielding to a decrease of the small-signal dielectric constant.[9] From our in situ TEM observations (Figs. 2 and 3), growths of relatively large domains were generally observed. Since the domain density of the fatigued state did not show a notable increase, and also a substantial degradation of dielectric constant occurred after fatigue [Fig. 5(b)], it seems to suggest a leading contribution from the seed inhibition mechanism. Here, it should be pointed out that the electrode degradation and passive layer formation models are not necessarily contradictory to the seed inhibition mechanism. According to Lou et al.,[50] the disappearance of the interface nucleation sites may be resulted from the growth of interfacial layer after fatigue.

Lastly, it should be stressed that other factors may also contribute to polarization fatigue, for example, cycling-induced microcracks, and the internal bias field from charge-accumulation at grain boundaries.[1,9,10] Since such effects are always manifested beyond individual grains they are beyond the primary focus of the present work at the individual grain level.

IV. CONCLUSIONS

In conclusion, an electric field in situ TEM study was conducted to investigate the microstructural origin for electric fatigue in the 0.7PMN-0.3PT ceramic. The domain evolution within individual grains was directly visualized during the fatigue process. The in situ observations correlated well with the macroscopic property measurements on bulk specimens. It was found that the fatigue behavior in this composition was due to the frozen domain configuration after 10^3 cycles, yielding to a progressive degradation of polarization, dielectric constant, and piezoelectric coefficient. Both microscopic and macroscopic observations suggested the seed inhibition as the primary mechanism for the resulted fatigue behaviors. The electric field in situ TEM technique used in this study was demonstrated to be a powerful and promising probing tool to reveal the underlying mechanism with microscopic insight for electric fatigue.

ACKNOWLEDGMENT

The National Science Foundation (NSF), through Grant DMR-1037898, supported this work.

REFERENCES

1. D.C. Lupascu: *Fatigue in Ferroelectric Ceramics and Related Issues* (Springer, Heidelberg, 2004).
2. J.F. Scott: *Ferroelectric Memories* (Springer, Berlin, 2000).
3. S. Mathews, R. Ramesh, T. Venkatesan, and J. Benedetto: Ferroelectric field effect transistor based on epitaxial perovskite heterostructures. *Science* **276**, 238 (1997).
4. S.H. Baek, H.W. Jang, C.M. Folkman, Y.L. Li, B. Winchester, J.X. Zhang, Q. He, Y.H. Chu, C.T. Nelson, M.S. Rzchowski, X.Q. Pan, R. Ramesh, L.Q. Chen, and C.B. Eom: Ferroelastic switching for nanoscale non-volatile magnetoelectric devices. *Nat. Mater.* **9**, 309 (2010).
5. S.D. Bernstein, T.Y. Wong, Y. Kisler, and R.W. Tustison: Fatigue of ferroelectric $PbZr_xTi_yO_3$ capacitors with Ru and RuO_x electrodes. *J. Mater. Res.* **8**(1), 12 (1993).
6. P. Maksymovych, S. Jesse, P. Yu, R. Ramesh, A.P. Baddorf, and S.V. Kalinin: Polarization control of electron tunneling into ferroelectric surfaces. *Science* **324**, 1421 (2009).
7. D.C. Lupascu and J. Rödel: Fatigue in bulk lead zirconate titanate actuator materials. *Adv. Eng. Mater.* **7**(10), 882 (2005).
8. S-H. Kim, J.G. Hong, S.K. Streiffer, and A.I. Kingon: The effect of RuO_2/Pt hybrid bottom electrode structure on the leakage and fatigue properties of chemical solution derived $Pb(Zr_xTi_{1-x})O_3$ thin films. *J. Mater. Res.* **14**(3), 1018 (1999).
9. A.K. Tagantsev, I. Stolichnov, E.L. Colla, and N. Setter: Polarization fatigue in ferroelectric films: Basic experimental findings, phenomenological scenarios, and microscopic features. *J. Appl. Phys.* **90**, 1387 (2001).
10. X.J. Lou: Polarization fatigue in ferroelectric thin films and related materials. *J. Appl. Phys.* **105**, 024101 (2009).
11. P.K. Larsen, G.J.M. Dormans, D.J. Taylor, and P.J. van Veldhoven: Ferroelectric properties and fatigue of $Pb_{0.51}Ti_{0.49}O_3$ thin films of varying thickness: Blocking layer model. *J. Appl. Phys.* **76**, 2405 (1994).
12. E.L. Colla, A.K. Tagantsev, D.V. Taylor, and A.L. Kholkin: Fatigued state of Pt-PZT-Pt system. *Integr. Ferroelectr.* **18**, 19 (1997).
13. W.L. Warren, D. Dimos, B.A. Tuttle, G.E. Pike, R.W. Schwartz, P.J. Clews, and D.C. McIntyre: Polarization suppression in Pb(Zr, Ti)O_3 thin films. *J. Appl. Phys.* **77**, 6695 (1995).
14. X.J. Lou, M. Zhang, S.A.T. Redfern, and J.F. Scott: Local phase decomposition as a cause of polarization fatigue in ferroelectric thin films. *Phys. Rev. Lett.* **97**, 177601 (2006).
15. S-H. Kim, D-J. Kim, J.G. Hong, S.K. Streiffer, and A.I. Kingon: Imprint and fatigue properties of chemical solution derived $Pb_{1-x}La(Zr_yTi_{1-y})_{1-x/4}O_3$ thin films. *J. Mater. Res.* **14**(4), 1371 (1999).
16. S.R. Shannigrahi, S-H. Lee, and H.M. Jang: Fatigue-free La-modified Pb(Zr, Ti)O_3 capacitors using a seed layer. *J. Mater. Res.* **17**(8), 1884 (2002).
17. X. Zou, L. You, W. Chen, H. Ding, D. Wu, T. Wu, L. Chen, and J. Wang: Mechanism of polarization fatigue in $BiFeO_3$. *ACS Nano* **6**(10), 8997 (2012).
18. S.M. Yang, T.H. Kim, J-G. Yoon, and T.W. Noh: Nanoscale observation of time-dependent domain wall pinning as the origin of polarization fatigue. *Adv. Funct. Mater.* **22**(11), 2310 (2012).
19. S-H. Baek, C.M. Folkman, J-W. Park, S. Lee, C-W. Bark, T. Tybell, and C-B. Eom: The nature of polarization fatigue in $BiFeO_3$. *Adv. Mater.* **23**(14), 1621 (2011).
20. A. Gruverman, O. Auciello, and H. Tokumoto: Nanoscale investigation of fatigue effects in Pb(Zr, Ti) films. *Appl. Phys. Lett.* **69**, 3191 (1996).

21. E.L. Colla, S. Hong, D.V. Taylor, A.K. Tagantsev, N. Setter, and K. No: Direct observation of region by region suppression of the switchable polarization (fatigue) in Pb(Zr, Ti)O_3 thin film capacitors with Pt electrodes. *Appl. Phys. Lett.* **72**, 2763 (1998).
22. E.L. Colla, I. Stolichnov, P.E. Bradely, and N. Setter: Direct observation of inversely polarized frozen nanodomains in fatigued ferroelectric memory capacitors. *Appl. Phys. Lett.* **82**, 1604 (2003).
23. S. Tsurekawa, H. Hatao, H. Takahashi, and Y. Morizono: Changes in ferroelectric domain structure with electric fatigue in $Li_{0.06}(Na_{0.5}K_{0.5})_{0.94}NbO_3$ ceramics. *Jpn. J. Appl. Phys.* **50**, 09NC02 (2011).
24. D-H. Do, P.G. Evans, E.D. Isaacs, D.M. Kim, C.B. Eom, and E.M. Dufresne: Structural visualization of polarization fatigue in epitaxial ferroelectric oxide devices. *Nat. Mater.* **3**, 365 (2004).
25. H.Z. Guo, S.J. Zhang, S.P. Beckman, and X. Tan: Microstructural origin for the piezoelectricity evolution in $(K_{0.5}Na_{0.5})NbO_3$-based lead-free ceramics. *J. Appl. Phys.* **114**, 154102 (2013).
26. X. Tan, C. Ma, J. Frederick, S. Beckman, and K.G. Webber: The antiferroelectric ↔ ferroelectric phase transition in lead-containing and lead-free perovskite ceramics. *J. Am. Ceram. Soc.* **94**(12), 4091 (2011).
27. C. Ma, H.Z. Guo, S.P. Beckman, and X. Tan: Creation and destruction of morphotropic phase boundaries through electrical poling: A case study of lead-free $(Bi_{1/2}Na_{1/2})TiO_3$–$BaTiO_3$ piezoelectrics. *Phys. Rev. Lett.* **109**, 107602 (2012).
28. S.E. Young, H.Z. Guo, C. Ma, M.R. Kessler, and X. Tan: Thermal analysis of phase transitions in perovskite electroceramics. *J. Therm. Anal. Calorim.* **115**(1), 587 (2014).
29. H.Z. Guo, C. Zhou, X. Ren, and X. Tan: Unique single-domain state in a polycrystalline ferroelectric ceramic. *Phys. Rev. B* **89**, 100104(R) (2014).
30. W. Qu, X. Zhao, and X. Tan: Evolution of nanodomains during the electric-field-induced relaxor to normal ferroelectric phase transition in a Sc-doped Pb ($Mg_{1/3}Nb_{2/3}$)O_3 ceramic. *J. Appl. Phys.* **102**, 084101 (2007).
31. X. Tan, H. He, and J.K. Shang: In situ transmission electron microscopy studies of electric-field-induced phenomena in ferroelectrics. *J. Mater. Res.* **20**(7), 1641 (2005).
32. H. Guo, C. Ma, X.M. Liu, and X. Tan: Electrical poling below coercive field for large piezoelectricity. *Appl. Phys. Lett.* **102**, 092902 (2013).
33. X. Tan and J.K. Shang: In situ transmission electron microscopy study of electric-field-induced grain-boundary cracking in lead zirconate titanate. *Philos. Mag. A* **82**(8), 1463 (2002).
34. H. He and X. Tan: Electric-field-induced transformation of incommensurate modulations in antiferroelectric $Pb_{0.99}Nb_{0.02}[(Zr_{1-x}Sn_x)_{1-y}Ti_y]_{0.98}O_3$. *Phys. Rev. B* **72**, 024102 (2005).
35. X. Tan, Z. Xu, J.K. Shang, and P. Han: Direct observations of electric field-induced domain boundary cracking in <001> oriented piezoelectric Pb($Mg_{1/3}Nb_{2/3}$)O_3-$PbTiO_3$ single crystal. *Appl. Phys. Lett.* **77**, 1529 (2000).
36. H. Wang, B. Jiang, T.R. Shrout, and W. Cao: Electromechanical properties of fine-grain 0.7Pb ($Mg_{1/3}Nb_{2/3}$)O_3-0.3$PbTiO_3$. *IEEE Trans. Ultrason. Ferroelectr., Freq. Control* **51**(7), 908 (2004).
37. R.M. McMeeking: Electrostrictive stresses near crack-like flaw. *J. Appl. Math. Phys.* **40**(5), 615 (1989).
38. D. Viehland, J. Li, and E.V. Colla: Domain structure changes in (1-x)Pb($Mg_{1/3}Nb_{2/3}$)O_3-x$PbTiO_3$ with composition, dc bias, and ac field. *J. Appl. Phys.* **96**(6), 3379 (2004).
39. F. Bai, J. Li, and D. Viehland: Domain engineered states over various length scales in (001)-oriented Pb($Mg_{1/3}Nb_{2/3}$)O_3-x%PbTiO3 crystals: Electrical history dependence of hierarchal domains. *J. Appl. Phys.* **97**, 054103 (2005).
40. H. Wu, D. Xue, D. Lv, J. Gao, S. Guo, Y. Zhou, X. Ding, C. Zhou, S. Yang, Y. Yang, and X. Ren: Microstructure at morphotropic phase boundary in Pb($Mg_{1/3}Nb_{2/3}$)O_3-$PbTiO_3$ ceramic: Coexistence of nano-scaled {110}-type rhombohedral twin and {110}-type tetragonal twin. *J. Appl. Phys.* **112**, 052004 (2012).
41. B. Noheda, D.E. Cox, G. Shirane, J. Gao, and Z-G. Ye: Phase diagram of the ferroelectric relaxor (1-x)Pb($Mg_{1/3}Nb_{2/3}$)O_3-x$PbTiO_3$. *Phys. Rev. B* **66**, 054104 (2002).
42. H. Wang, J. Zhu, N. Lu, A.A. Bokov, Z-G. Ye, and X.W. Zhang: Hierarchical micro-/nanoscale domain structure in MC phase of (1-x)Pb($Mg_{1/3}Nb_{2/3}$)O_3-xPbTiO3 single crystal. *Appl. Phys. Lett.* **89**, 042908 (2006).
43. Y. Sato, T. Hirayama, and Y. Ikuhara: Monoclinic nanodomains in morphotropic phase boundary Pb($Mg_{1/3}Nb_{2/3}$)O_3-$PbTiO_3$. *Appl. Phys. Lett.* **104**, 082905 (2014).
44. K. Kurushima, K. Kobayashi, and S. Mori: Nanodomain structures with hierarchical inhomogeneities in PMN-PT. *IEEE Trans. Ultrason. Ferroelectr., Freq. Control* **59**(9), 1900 (2012).
45. M. Dawber and J.F. Scott: A model for fatigue in ferroelectric perovskite thin films. *Appl. Phys. Lett.* **76**(8), 1060 (2000).
46. D.C. Lupascu and U. Rabe: Cyclic cluster growth in ferroelectric perovskites. *Phys. Rev. Lett.* **89**(18), 187601 (2002).
47. C-C. Chou, C-S. Hou, and T-H. Yeh: Domain pinning behavior of ferroelectric $Pb_{1-x}Sr_xTiO_3$ ceramics. *J. Eur. Ceram. Soc.* **25**, 2505 (2005).
48. C-C. Chou, C-S. Hou, and H-C. Pan: Domain boundary pinning and nucleation of ferroelectric $(Pb_{1-x}Sr_x)TiO_3$ ceramics. *Ferroelectrics* **261**, 185 (2001).
49. J.J. Lee, C.L. Thio, and S.B. Desu: Electrode contacts on ferroelectric Pb(Zr_xTi_{1-x})O_3 and $SrBi_2Ta_2O_9$ thin films and their influence on fatigue properties. *J. Appl. Phys.* **78**, 5073 (1995).
50. X.J. Lou and J. Wang: Bipolar and unipolar electrical fatigue in ferroelectric lead zirconate titanate thin films: An experimental comparison study. *J. Appl. Phys.* **108**, 034104 (2010).
51. X.J. Lou and J. Wang: Unipolar and bipolar fatigue in antiferroelectric lead zirconate thin films and evidences for switching-induced charge injection inducing fatigue. *Appl. Phys. Lett.* **96**, 102906 (2010).
52. E.L. Colla, A.L. Kholkin, D. Taylor, A.K. Tagantsev, K.G. Brooks, and N. Setter: Characterization of the fatigued state of ferroelectric PZT thin-film capacitors. *Microelectron. Eng.* **29**, 145 (1995).
53. C. Thompson, A. Munkholm, S.K. Streiffer, G.B. Stephenson, K. Ghosh, J.A. Eastman, O. Auciello, G-R. Bai, M.K. Lee, and C.B. Eom: X-ray scattering evidence for the structural nature of fatigue in epitaxial Pb(Zr,Ti)O_3 films. *Appl. Phys. Lett.* **78**, 3511 (2001).
54. L.F. Schloss and P.C. Mclntyre: Polarization recovery of fatigued Pb(Zr,Ti)O_3 thin films: Switching current studies. *J. Appl. Phys.* **93**, 1743 (2003).
55. F. Kubel and H. Schmid: Structure of a ferroelectric and ferroelastic monodomain crystal of the perovskite $BiFeO_3$. *Acta Crystallogr., B* **46**, 698 (1990).
56. J.E. Daniels, T.R. Finlayson, M. Davis, D. Damjanovic, A.J. Studer, M. Hoffman, and J.L. Jones: Neutron diffraction study of the polarization reversal mechanism in $[111]_C$-oriented Pb($Zn_{1/3}Nb_{2/3}$)O_3-$x$$PbTiO_3$. *J. Appl. Phys.* **101**, 104108 (2007).
57. W. Zhu and L.E. Cross: Direct evidence of ferroelastic participation in 180° polarization switching and fatigue for 111 oriented rhombohedral ferroelectric 0.955 Pb($Zn_{1/3}Nb_{2/3}$)O_3:0.045$PbTiO_3$ single crystals. *Appl. Phys. Lett.* **84**, 2388 (2004).
58. C-Y. Hsieh, Y-F. Chen, W.Y. Shih, Q. Zhu, and W-H. Shih: Direct observation of two-step polarization reversal by an opposite field in a substrate-free piezoelectric thin sheet. *Appl. Phys. Lett.* **94**, 131101 (2009).

59. W. Cao: Switching mechanism in single crystal $0.955Pb(Zn_{1/3}Nb_{2/3})O_3$-$0.045PbTiO_3$. *Ferroelectrics* **290**, 107 (2003).
60. Y. Kitanaka, K. Yanai, Y. Noguchi, M. Miyayama, Y. Kagawa, C. Moriyoshi, and Y. Kuroiwa: Non-180° polarization rotation of ferroelectric $(Bi_{0.5}Na_{0.5})TiO_3$ single crystals under electric field. *Phys. Rev. B* **89**, 104104 (2014).
61. V.Y. Shur, A.R. Akhmatkhanov, and I.S. Baturin: Fatigue effect in ferroelectric crystals: Growth of the frozen domains. *J. Appl. Phys.* **111**, 124111 (2012).